ADVANCED MATERIALS

www.advmat.de

Magnetically Addressable Shape-Memory and Stiffening in a Composite Elastomer

Paolo Testa, Robert W. Style, Jizhai Cui, Claire Donnelly, Elena Borisova, Peter M. Derlet, Eric R. Dufresne,* and Laura J. Heyderman**

With a specific stimulus, shape-memory materials can assume a temporary shape and subsequently recover their original shape, a functionality that renders them relevant for applications in fields such as biomedicine, aerospace, and wearable electronics. Shape-memory in polymers and composites is usually achieved by exploiting a thermal transition to program a temporary shape and subsequently recover the original shape. This may be problematic for heat-sensitive environments, and when rapid and uniform heating is required. In this work, a soft magnetic shape-memory composite is produced by encasing liquid droplets of magneto-rheological fluid into a poly(dimethylsiloxane) matrix. Under the influence of a magnetic field, this material undergoes an exceptional stiffening transition, with an almost 30-fold increase in shear modulus. Exploiting this transition, fast and fully reversible magnetic shape-memory is demonstrated in three ways, by embossing, by simple shear, and by unconstrained 3D deformation. Using advanced synchrotron X-ray tomography techniques, the internal structure of the material is revealed, which can be correlated with the composite stiffening and shape-memory mechanism. This material concept, based on a simple emulsion process, can be extended to different fluids and elastomers, and can be manufactured with a wide range of methods.

Shape-memory materials can assume a temporary shape through a programming step and can then recover their original shape in response to a specific stimulus.[1] By encoding mechanical functionality in the material itself, rather than in the device, these materials allow for a reduction in the complexity of parts and an increase in energy efficiency.[2] Compared to other classes of shape-memory materials, shape-memory polymers and composites are lightweight, inexpensive, can be made into parts using a variety of manufacturing technologies, and can have a broad range of properties.[3] Thanks to these characteristics, they find applications in a variety of engineering areas including aerospace,[4] wearable electronics,[5] and biomedicine.[6] The design of shape-memory polymers is usually based on the combination of two distinct phases, a stable phase and a programmable phase. The programmable phase can undergo a reversible stiffening transition triggered by an external stimulus, while the stable phase remains unaffected. If the programmable phase is stiffer than the stable phase, the material can hold a temporary shape, while the inverse transition leads to the recovery of the original shape.[7] Typically, the change in stiffness of the programmable phase is achieved through a thermally induced phase transition.[8] Heating of the material, however, can be nonuniform and slow, since polymers are relatively good heat insulators.[9,10] Additionally, the use of thermal stimuli greatly limits applications in heat-sensitive environments such as the human body, as heat can harm living tissues.[11,12] Therefore, when considering biomedical applications, careful tuning of the shape recovery temperature is required for safe employment of these materials since triggering temperatures above body temperature can cause cell damage while, for activation temperatures below body temperature, the effect may be triggered prematurely.[13]

Here, we present an athermal, magnetically addressable shape-memory polymer composite, produced by dispersing droplets of a commercial magneto-rheological fluid in a crosslinked poly(dimethylsiloxane) (PDMS) matrix, shown schematically in **Figure 1**a. Magneto-rheological fluids are able to undergo a substantial change at the millisecond timescale when subjected to a magnetic field, with mechanical properties such as viscosity, shear modulus, and yield stress increasing by up to six orders of magnitude.[14,15] By encasing the magneto-rheological fluid in an elastomeric matrix, we are able to manufacture a soft elastic composite with exceptional

P. Testa, Dr. J. Cui, Dr. C. Donnelly, Prof. L. J. Heyderman
Laboratory for Mesoscopic Systems
Department of Materials
ETH Zurich
8093 Zurich, Switzerland
E-mail: paolo.testa@mat.ethz.ch; laura.heyderman@psi.ch

P. Testa, Dr. R. W. Style, Prof. E. R. Dufresne
Laboratory for Soft and Living Materials
Department of Materials
ETH Zurich
8093 Zurich, Switzerland
E-mail: eric.dufresne@mat.ethz.ch

P. Testa, Dr. J. Cui, Dr. C. Donnelly, Dr. E. Borisova,
Dr. P. M. Derlet, Prof. L. J. Heyderman
Paul Scherrer Institute
5232 Villigen, Switzerland

The ORCID identification number(s) for the author(s) of this article can be found under https://doi.org/10.1002/adma.201900561.

DOI: 10.1002/adma.201900561

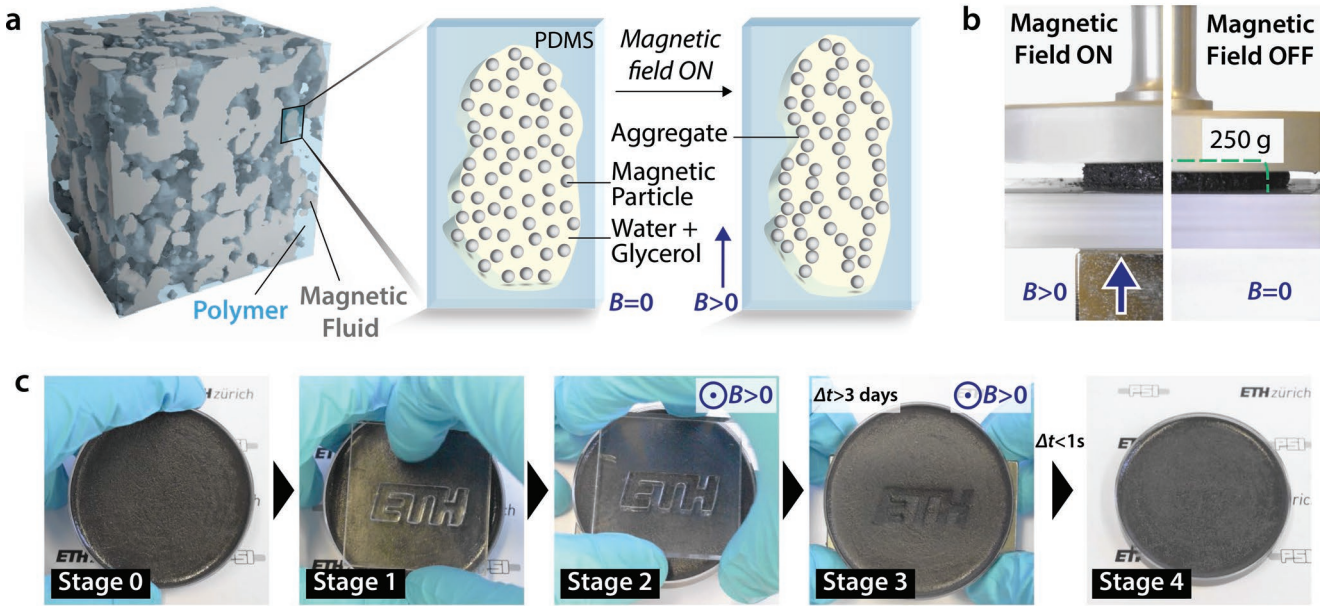

Figure 1. Magnetically addressable stiffening and shape-memory in a polymer/magneto-rheological fluid composite. a) 3D reconstruction of the internal structure of the material obtained from tomography data, providing a 3D visualization of the two different phases in the composite (cube edge = 390 µm). The effect of the magnetic field on the internal structure of the magnetic phase in a droplet is schematically shown. With no magnetic field applied, the carbonyl iron microparticles are uniformly dispersed in the carrier solvent, consisting of water and glycerol, and the droplet is in a liquid state. After the application of a magnetic field, the particles rearrange to align with the field, resulting in a stiffness increase of several orders of magnitude in the magnetic fluid. b) Experimental demonstration of the influence of the magnetic field on the stiffness of the material. A disk of material is able to carry a weight of 250 g when subjected to a magnetic field from a permanent magnet (left), while it becomes soft and compliant under the same weight when the magnet is removed (right). c) Embossing a disk of material demonstrating magnetic shape-memory. The material can be programmed to retain a certain shape in a magnetic field, and returns to the original shape after removal of the field. A disk of material (initial Stage 0) is embossed using a stamp with a defined profile (Stage 1) and subsequently an out-of-plane magnetic field is applied with a permanent magnet (Stage 2). The material retains the programmed shape for several days (Stage 3) until the magnetic field is removed, after which it returns to the original shape in less than 1 s (Stage 4). Images are taken from Movie S1 available in the Supporting Information.

magneto-mechanical properties. The composite can undergo substantial stiffening when subjected to a magnetic field, with an exceptional increase in storage modulus of approximatively thirty times at a field of 600 mT (see **Figures** 1b and 2e). In addition, the composite displays magnetically addressable shape-memory, where the PDMS matrix acts as the stable phase and the magnetic fluid as the programmable phase. An applied deformation can be programmed in the composite through the application of a magnetic field. The composite relaxes back to its original form in less than 1 s when the magnetic field is released, as shown in Figure 1c and in the Movie S1 available in the Supporting Information. The combination of various types of liquid inclusions with soft elastomeric matrices has been recently proposed as an effective way to create soft materials with novel functionalities, such as high electrical conductivity and temperature dependent color.[16–19] We have extended this approach to our material, using instead a magneto-rheological fluid. This has a number of advantages compared to previously reported composites in which the magnetic particles are directly dispersed in the polymer matrix.[20,21] Due to the larger mobility of the particles when suspended in a liquid solvent, the alignment of particles that causes the mechanical property change becomes more effective, resulting in a larger stiffening effect. At the same time, the degradation of mechanical properties often observed with soft composites with incorporated hard particles, such as embrittlement and reduced durability, is avoided, thanks to the liquid nature of the magnetic component.[22]

We dispersed magneto-rheological fluid droplets in PDMS prior to crosslinking at volume fractions, ϕ, ranging from 0% to 40%, as described in the Experimental Section. In order to understand the effect of the magnetic field on the microstructure of the material, we used X-ray tomographic imaging to assess the internal structure of the composite at length scales from ≈3 µm up to 1 mm. In this range, we can resolve the shape and internal structure of the droplets as well as their arrangement in the elastic matrix (full tomographic reconstructions of the composite structure, with and without the applied field, are available as Movies S2 and S3 in the Supporting Information). A 3D rendering of the tomographic reconstruction for a composite with ϕ = 40% at B = 0 mT is shown in Figure 1a, with a single 2D slice shown in Figure 2a. The highly X-ray absorbing iron particles inside the fluid are recognizable as dark gray regions, while the X-ray transparent silicone and solvent, consisting of a water and glycerol mixture, are essentially indistinguishable from each other. The single iron particles in the magnetic fluid have sizes in the range of 1 to 6 µm (see Figures S1 and S2 in the Supporting Information), which is at the spatial resolution limit of the tomographic imaging tool. Although the single particles are not resolvable, the general microparticle distribution can be assessed and, when the sample is not subjected to a magnetic field, both the droplet

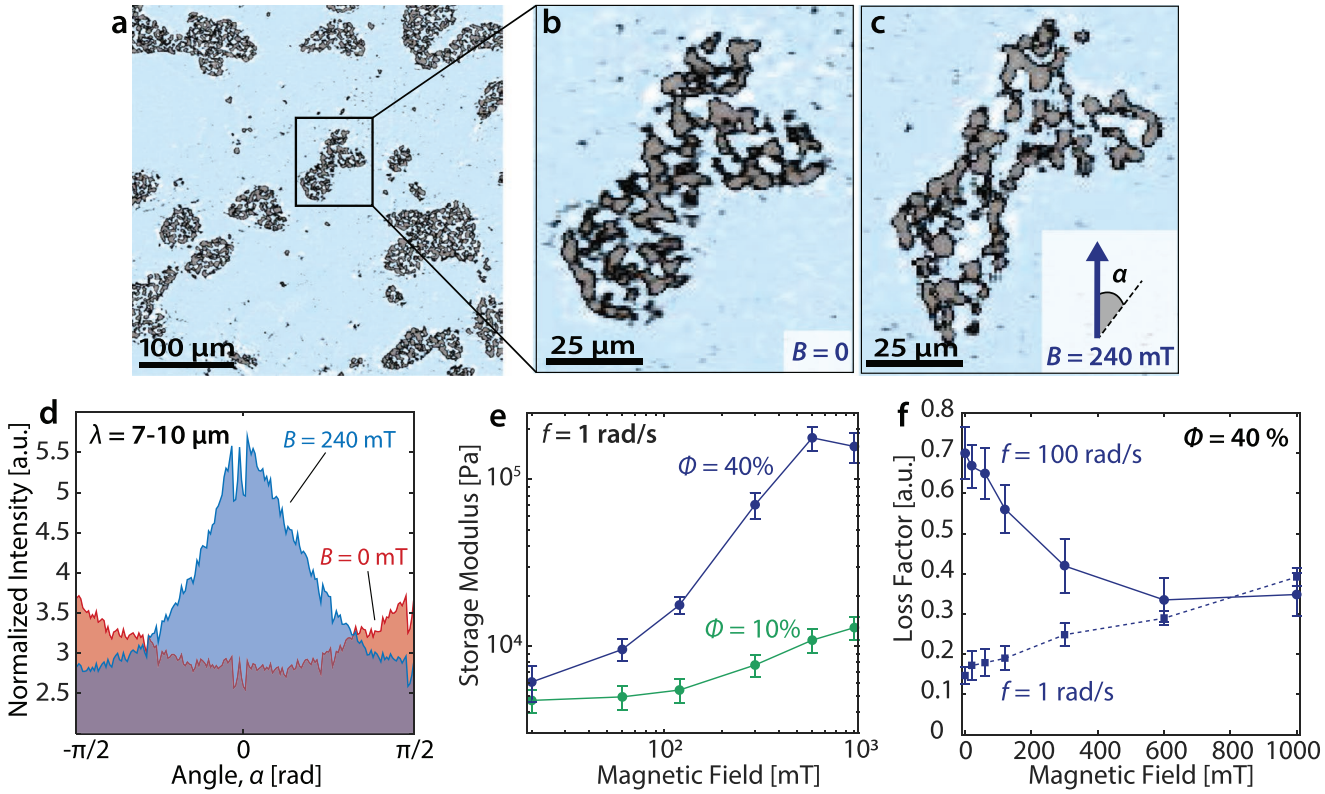

Figure 2. Effect of the magnetic field on the structure and properties of the composite elastomer. a) 2D slice of an X-ray absorption tomogram, obtained for a composite with $\phi = 40\%$ and with no magnetic field applied. The iron particles, in gray, can be distinguished from the rest of the components, in light blue. b) Close-up view of a single aggregate from the slice in (a). c) The same aggregate in (b) after the application of a magnetic field of 240 mT, demonstrating the rearrangement of the iron particles with droplet elongation in the direction of the applied field. d) Azimuthal plot of the normalized, average fast Fourier transform intensity for complete tomographic stacks of the same sample taken at fields of $B = 0$ and 240 mT. The plot refers to data in a wavelength range, $\lambda = 7$–10 μm, corresponding to the length scale of the magnetic particles in the fluid. The emergence of a peak after the application of the magnetic field in the vicinity of $\alpha = 0$ indicates that the magnetic particles inside the fluid droplets orient along the field direction. e) Magnetic-field-induced change in the storage modulus for $\phi = 10\%$ and 40%. Higher stiffening is observed for larger ϕ. f) Change in the loss factor at frequencies of $f = 1$ and 100 rad s^{-1} with magnetic field for a composite with $\phi = 40\%$.

shape and internal particle arrangement show no preferential orientation (Figure 2b). On application of a magnetic field, the microstructure changes, with both the droplet elongating and the particles inside the droplets aligning in the direction of the field (Figure 2c). To verify the observed alignment, we performed Fourier analysis of the 3D reconstructed structure, and analyzed the angular dependence of the Fourier transform intensity (for details of the analysis, see the Supporting Information). The angle α, shown in Figure 2c, indicates a specific orientation relative to the direction of the magnetic field. When the magnetic field is applied, we see an enhancement of the Fourier transform intensity at an orientation parallel to the field, indicating that the magnetic particles inside the fluid droplets orient along the field direction (see Figure 2d for an azimuthal representation and Figure S5 in the Supporting Information for the Fourier transform spectra). This feature is prominent for several different wavelengths in the range 5–100 μm (see Figure S6 in the Supporting Information), which are comparable to the size of the magnetic particles (≈1 to 6 μm) and the magnetic fluid droplets (≈20 to 100 μm). We further quantified the alignment by analyzing the angular dependence of the Fourier transform intensity in the region between $\alpha = 0$ and $\alpha = \pi/2$ and calculating the orientation order parameter S, which describes the average orientation of the structure with respect to the magnetic field direction (for details on the calculation, see the Supporting Information). S can assume values between approximately 0, meaning no preferential orientation, and 1, representing complete ordering. The value of S when no magnetic field is applied is small and negative, suggesting that the structure has no preferential orientation. After the application of the magnetic field, S is equal to 0.54, which implies a partial orientation of the structure along the field direction.

The alignment of the microstructure in the magnetic field direction observed with the tomographic analysis has a dramatic impact on the composite rheology. In order to determine the extent of this modification to the rheological properties, we measured the magneto-rheological response of the material in shear using a parallel plate rheometer equipped with a magnetic field generator, with the field-direction perpendicular to the plate surface. Frequency sweep data for the base components and for two composites with volume fractions, $\phi = 10\%$ and 40%, are available in Figure S8, with field-dependent rheological properties for all compositions in

Figure S9, in the Supporting Information. The magnetic field dependence of the storage modulus for these two different values of ϕ is shown in Figure 2e. At a relatively low volume fraction, ϕ = 10%, the storage modulus of the composite increases almost twofold with application of a 1000 mT field. At ϕ = 40%, the same magnetic field results in an almost 30-fold increase in the storage modulus. These values are remarkably high compared to previous results obtained for composites with magnetic particles dispersed directly in PDMS matrices where storage moduli increases of only 1.3–1.8 fold were reported at significantly higher iron contents.[23] The dissipative behavior of the material is also affected by the magnetic field (Figure 2f; Figure S9b, Supporting Information), with the highest change in loss factor with field observed in a composite with ϕ = 40% (Figure 2f). Indeed, the loss factor displays a total decrease of 50% on application of a magnetic field of 1000 mT for high frequencies (100 rad s^{-1}), and a twofold increase at the same field for low frequencies (1 rad s^{-1}). This change in the loss factor with magnetic field is much more significant than that previously reported for composites with magnetic particles dispersed in polymer matrices,[24] and is relevant for applications requiring adaptive vibration damping.[25]

We have seen how the magnetic field has a significant effect on the mechanical properties of the material. We additionally determined how the volume fraction of the magneto-rheological fluid, ϕ, influences the spatial arrangement of the different phases in the composite and how this, in turn, affects the magneto-mechanical properties of the material. We, therefore, measured the mechanical properties of the composite for different ϕ, with the storage modulus G' versus ϕ shown in **Figure 3**a. It can be seen that, at a field of 1000 mT, the storage modulus increases with ϕ, with a steep increase above ϕ = 20%. This suggests a corresponding change in the spatial arrangement of the magnetic fluid droplets with increasing ϕ, which we characterized with X-ray tomography (for details of the analysis, see the Supporting Information). In particular, we quantified the connectivity of the magnetic fluid droplet network using an order parameter, P, which is a measure of the ratio of the volume of magnetorheological fluid in the largest droplet to the total volume of the magnetorheological fluid in the observed tomography region. As shown in Figure 3b, the connectivity increases sharply at ϕ > 20% and, at this volume fraction, the droplets of magnetic fluid form a fully connected network above the percolation threshold.[26] This confirms that the sharp change in mechanical properties is linked to an abrupt microstructural transformation,[27] and this change in connectivity can be seen in the 3D reconstruction of the internal structure (Figure 3c).

We now demonstrate that the composite possesses a magnetically addressable shape-memory. This effect was quantified via the application of the controlled shear stress and magnetic field protocol shown in **Figure 4**a, employing the same rheometer used for the mechanical characterization. This measurement is analogous to the actions performed on a strip of material, shown in Figure 4b and Movie S4 available in the Supporting Information. Initially, the composite is in its original stress-free state (Initial Stage 0). Upon application of external stress, the entire composite deforms into a temporary shape. Here, the elastomeric component of the composite develops a restoring stress, while the droplets in their liquid state remain stress-free (Stage 1). Upon application of a uniform magnetic field, the droplets solidify in a nearly stress-free state, while the continuous phase is unaffected (Stage 2). When the external stress is released, the restoring stress in the polymer network is counteracted by the stiffness of the droplet phase. If the yield stress of the droplet phase is much larger than the stresses in the polymer network, the polymer network achieves only a partial elastic recovery, in this case only 10%, and the material retains a profile close to its programmed shape (Stage 3). When the magnetic field is removed, the droplets fluidize, allowing the elastomer to return to its original remembered shape (Stage 4). After this last step, a new cycle can be repeated, as the shape-memory is completely rewritable.

In conclusion, we have presented a composite displaying unique magneto-mechanical properties, with an athermal, fast shape-memory and up to an almost 30-fold stiffening. Using advanced tomography methods, we correlated these

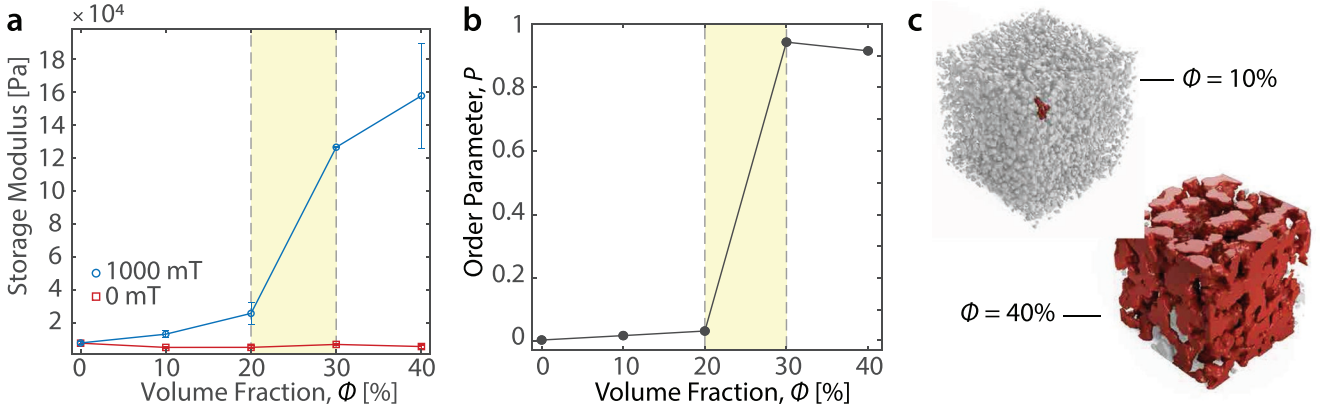

Figure 3. Effect of the fluid volume fraction on the stiffness and structure of the material. a) Dependence of the storage modulus on the droplet volume fraction, ϕ. The blue (red) points are data for an applied magnetic field of 1000 mT (0 mT). A sharp increase in the storage modulus is observed at ϕ > 20%, corresponding to a change in the spatial arrangement of the phases. b) Increase of connectivity with ϕ, quantified by the order parameter, P. The sharp increase of the value of P at ϕ > 20% indicates the onset of a fully connected magnetic fluid network, which, in turn, results in the sharp change in mechanical properties shown in (a). c) 3D reconstruction of the internal structure of the material at ϕ = 10% and 40% (cube edge = 390 µm). Highlighted in red is the biggest aggregate in the analyzed volume, which visually shows that the network of magnetic fluid is completely connected for ϕ = 40%.

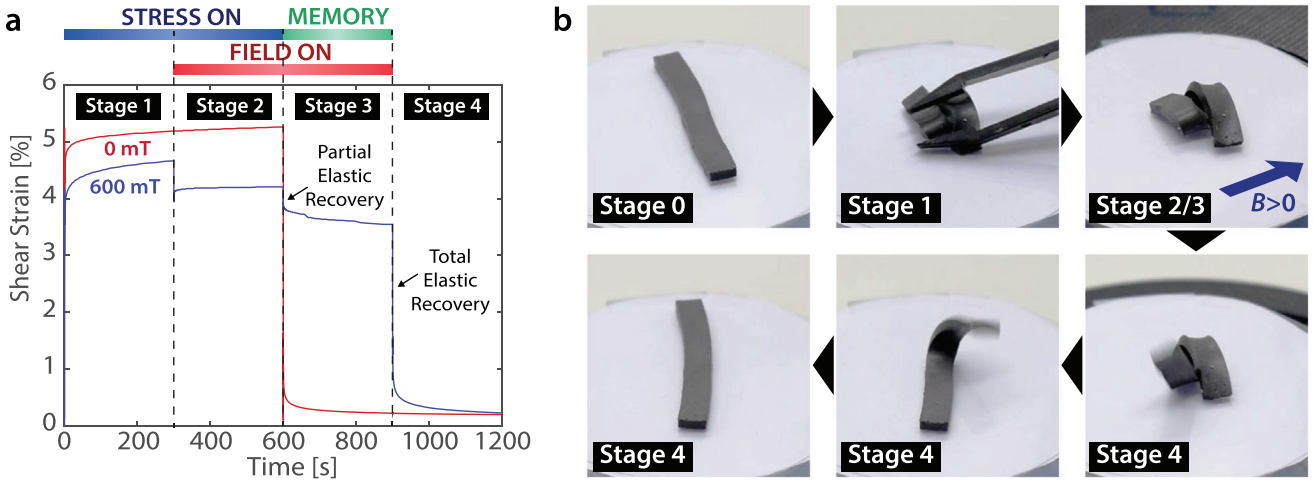

Figure 4. Magnetic shape-memory. a) Stepwise stress experiment performed in the absence (red curve) and the presence (blue curve) of a magnetic field. In zero field, the material recovers its original state once the stress is removed (Stage 2 to Stage 3). When a magnetic field of 600 mT is applied, the material retains almost all of the deformation (Stage 3), and recovers the original shape once the field is removed (Stage 4). b) Experimental demonstration of magnetic shape-memory in an unconstrained strip deformed in three dimensions. A 4 cm long strip can be deformed into an arbitrary shape, which is stabilized with a uniform magnetic field applied using an arrangement of permanent magnets (Stage 2/3). This programmed shape is retained until the magnetic field is removed and the strip returns to its remembered shape in a few seconds (Stage 4).The images are taken from Movie S4 available in the Supporting Information.

properties with the microstructural transformations induced by both the magnetic field and the volume fraction of magneto-rheological fluid. The fact that this shape-memory requires no heat, in conjunction with recent advances in magnetic control systems,[28] opens up new possibilities for applications such as biomedical and wearable devices, which are operated in heat-sensitive environments. Based on a straightforward emulsion process, this material composite can not only be extended to different classes of polymer matrices and active fluids, but can also be manufactured with a wide range of methods, including casting, injection molding, and additive manufacturing.[29]

Experimental Section

Fabrication of the Composite: A water-based magneto-rheological fluid (formulated on request, Liquids Research Limited) with 80% weight fraction of carbonyl iron microparticles was modified to avoid solvent evaporation by adding glycerol, resulting in a final fluid containing 66% weight fraction of iron microparticles, 17% weight fraction of glycerol, and 17% weight fraction of water and stabilizers. At a relative humidity of ≈40%, drying was not observed over the course of one week, as expected from the equilibrium composition of the water–glycerol mixture.[30] PDMS was obtained by mixing different ratios of vinyl-terminated PDMS (DMS-V31, Gelest Inc.) with (25–35% methylhydrosiloxane)-dimethylsiloxane copolymer, trimethylsiloxane terminated (HMS-301, Gelest Inc.), with the addition of platinum divinyl tetramethyldisiloxane catalyst (SIP6831.2, Gelest Inc.) according to the methodology reported by Style et al.[16] to obtain the desired elastic modulus. To form the liquid precursor emulsion for the final composite, appropriate ratios of fluid and PDMS were added together with the surfactant molecule PEG-dimethicone (ES5612, DOW Corning) and stirred manually for 5 min. This resulted in a water-in-oil emulsion driven by the demixing of the water-based magneto-rheological fluid and the silicone precursors. The emulsion was stabilized by the surfactant during polymerization. The mixture was degassed in a vacuum chamber for an additional 5 min and left to crosslink overnight at room temperature.

Supporting Information

Supporting Information is available from the Wiley Online Library or from the author.

Acknowledgements

Each author contributed to this work as follows: L.J.H. and P.M.D. conceived the project. P.T., E.R.D., and L.J.H. developed the material concept, with the help of R.W.S., P.T., and E.R.D. designed the magneto-mechanical measurements. P.T. and C.D. designed the tomography measurement. P.T. performed all measurements, with the help of C.D., J.C., and E.V.B. for the tomography measurement, and with the help of R.W.S. and E.R.D. for the magneto-mechanical measurements. P.T. and E.R.D. analyzed the data, with help from R.W.S., P.T., E.R.D., and L.J.H. wrote the manuscript, with help from all authors. The authors thank Jens Heller and Jonathan Halter for their help with initial tomography trials for the tomography beamtime proposal, the Complex Materials group at the Department of Materials at ETH Zurich for the use of their rheometer, Marius Wagner and Christian Furrer for their help with the realization of the tomography holder, and Valerio Scagnoli for his help with the interpretation of the Fourier transform plots. The authors additionally thank Andrea Testa, Laura Maurel, Qin Xu, Nicolas Bain, Dominic Gerber, and Alba Sicher for their help with the experimental work and useful discussions. The authors acknowledge the Paul Scherrer Institute, Villigen, Switzerland for provision of synchrotron radiation beamtime at the TOMCAT beamline X02DA of the SLS. This work was funded by an ETH Grant (Grant No. ETH-48 17-1 "Tailored mesoscopic magneto-mechanical systems," awarded for a project proposed by P.T., P.M.D., and L.J.H.). J.C. has received funding from the European Union's Horizon 2020 research and innovation program under the Marie Skłodowska-Curie grant agreement No. 701647. The raw data that supports this study is available via the Zenodo repository at https://doi.org/10.5281/zenodo.2842084.

Conflict of Interest

The authors declare no conflict of interest.

Keywords

liquid inclusions, magneto-mechanical materials, magneto-rheology, soft matter, X-ray tomography

Received: January 23, 2019
Revised: April 11, 2019
Published online: June 4, 2019

[1] A. Lendlein, S. Kelch, *Angew. Chem., Int. Ed.* **2002**, *41*, 2034.
[2] W. M. Huang, Z. Ding, C. C. Wang, J. Wei, Y. Zhao, H. Purnawali, *Mater. Today* **2010**, *13*, 54.
[3] W. Sokolowski, A. Metcalfe, S. Hayashi, L. Yahia, J. Raymond, *Biomed. Mater.* **2007**, *2*, S23.
[4] W. M. Sokolowski, A. B. Chmielewski, S. Hayashi, T. Yamada, in *Proc. SPIE 3669, Smart Struct. Mater.* (Ed: Y. Bar-Cohen), **1999**, pp. 179–185.
[5] M. Zarek, M. Layani, I. Cooperstein, E. Sachyani, D. Cohn, S. Magdassi, *Adv. Mater.* **2016**, *28*, 4166.
[6] A. Tonazzini, S. Mintchev, B. Schubert, B. Mazzolai, J. Shintake, D. Floreano, *Adv. Mater.* **2016**, *28*, 10142.
[7] M. D. Hager, S. Bode, C. Weber, U. S. Schubert, *Prog. Polym. Sci.* **2015**, *49–50*, 3.
[8] T. Xie, *Nature* **2010**, *464*, 267.
[9] W. Li, Y. Liu, J. Leng, *J. Mater. Chem. A* **2015**, *3*, 24532.
[10] J. M. Cuevas, J. Alonso, L. German, M. Iturrondobeitia, J. M. Laza, J. L. Vilas, L. M. León, *Smart Mater. Struct.* **2009**, *18*, 075003.
[11] C. Liu, H. Qin, P. T. Mather, *J. Mater. Chem.* **2007**, *17*, 1543.
[12] J. Ortega, D. Maitland, T. Wilson, W. Tsai, Ö. Savaş, D. Saloner, *Ann. Biomed. Eng.* **2007**, *35*, 1870.
[13] L. Yahia, in *Shape Memory Polymers for Biomedical Applications*, (Ed: L. Yahia), Woodhead Publishing, Cambridge, UK **2015**, pp. 3–8.
[14] S. Elizabeth Premalatha, R. Chokkalingam, M. Mahendran, *Am. J. Polym. Sci.* **2012**, *2*, 50.
[15] H. M. Laun, C. Gabriel, *Rheol. Acta* **2007**, *46*, 665.
[16] R. W. Style, R. Boltyanskiy, B. Allen, K. E. Jensen, H. P. Foote, J. S. Wettlaufer, E. R. Dufresne, *Nat. Phys.* **2015**, *11*, 82.
[17] N. Kazem, M. D. Bartlett, C. Majidi, *Adv. Mater.* **2018**, *30*, 1706594.
[18] D. Doblas, J. Hubertus, T. Kister, T. Kraus, *Adv. Mater.* **2018**, *30*, 1803159.
[19] J. A. Jackson, M. C. Messner, N. A. Dudukovic, W. L. Smith, L. Bekker, B. Moran, A. M. Golobic, A. J. Pascall, E. B. Duoss, K. J. Loh, C. M. Spadaccini, *Sci. Adv.* **2018**, *4*, eaau6419.
[20] G. Filipcsei, I. Csetneki, A. Szilágyi, M. Zrínyi, *Adv. Polym. Sci.* **2007**, *206*, 137.
[21] Y. Li, J. Li, W. Li, H. Du, *Smart Mater. Struct.* **2014**, *23*, 123001.
[22] M. D. Bartlett, A. Fassler, N. Kazem, E. J. Markvicka, P. Mandal, C. Majidi, *Adv. Mater.* **2016**, *28*, 3726.
[23] W. H. Li, M. Nakano, *Smart Mater. Struct.* **2013**, *22*, 055035.
[24] M. Kallio, *Doctoral Thesis*, Tampere University of Technology, Tampere, Finland **2005**.
[25] V. S. Molchanov, G. V. Stepanov, V. G. Vasiliev, E. Y. Kramarenko, A. R. Khokhlov, Z. D. Xu, Y. Q. Guo, *Macromol. Mater. Eng.* **2014**, *299*, 1116.
[26] M. D. Rintoul, S. Torquato, *J. Phys. A: Math. Gen.* **1997**, *30*, L585.
[27] A. K. Kota, B. H. Cipriano, M. K. Duesterberg, A. L. Gershon, D. Powell, S. R. Raghavan, H. A. Bruck, *Macromolecules* **2007**, *40*, 7400.
[28] J. Rahmer, C. Stehning, B. Gleich, *Sci. Rob.* **2017**, *2*, eaal2845.
[29] Y. Kim, H. Yuk, R. Zhao, S. A. Chester, X. Zhao, *Nature* **2018**, *558*, 274.
[30] *Physical Properties of Glycerol and Its Solutions*, Glycerine Producers' Association, New York **1953**.